Cryogenics 58 (2013) 78–84

Contents lists available at ScienceDirect

Cryogenics

journal homepage: www.elsevier.com/locate/cryogenics

Investigation on the generation mechanisms of acoustic streaming in a thermoacoustic prime mover

R. Paridaens, S. Kouidri *, F. Jebali Jerbi

LIMSI-CNRS, BP 133-91403 Orsay Cedex, France
UPMC Univ Paris 06, UFR 919, 4 place Jussieu, 75752 Paris Cedex 05, France

ARTICLE INFO

Article history:
Received 7 August 2013
Received in revised form 7 October 2013
Accepted 11 October 2013
Available online 26 October 2013

Keywords:
Thermoacoustics
Prime mover
Streaming

ABSTRACT

High-amplitude acoustic waves in thermoacoustic devices are responsible for the generation of a secondary flow called acoustic streaming. Superimposed on the oscillating flow, this secondary flow is an important source of energy dissipation. To remove acoustic streaming would result in substantial improvements in the energy performance of thermoacoustic devices. Understanding the control parameters and mechanisms of streaming generation is essential for controlling acoustic streaming.

In this paper, streaming sources are investigated in a pressurized thermoacoustic prime mover. The device was designed and built at the LIMSI (Laboratoire d'Informatique pour la Mécanique et les Sciences de l'Ingénieur) to investigate acoustic streaming. To calculate the theoretical velocity in the thermoacoustic device, the usual modelings were extended to take into account the cross section variation. Measurements of acoustic streaming velocity performed by Laser Doppler Velocimetry are compared to the theoretical results. Finally, the good agreements obtained led to the validation of the theory. The validated theory was then used to study the mechanisms of streaming generation in order to determine their influences in the thermoacoustic prime mover and therefore reducing the secondary flow. Thereafter, the investigation was extended to four channels with different widths and according to results of the literature, the proportion of outer streaming compared to inner streaming decreases when the channel width decrease. The investigation showed that the mechanisms of acoustic streaming generation differ for large and narrow channels.

© 2013 Elsevier Ltd. All rights reserved.

1. Introduction

In the energy transition century, thermoacoustic systems have been receiving a renewed interest. Thermoacoustic devices are a part of the cleanest energy conversion systems for the environment because they use non-polluting gases [1,2]. As thermoacoustic systems have no mechanical moving component, they are also highly reliable and have a long lifetime. To keep these reliable and environmental properties, pulse tube refrigerators could be driven by thermoacoustic engines [3–5]. Despite its strengths, energy efficiency of thermoacoustic devices is still low. Therefore, increasing the performance of these systems is an important issue in the thermoacoustic community [6–8]. The high mean pressure amplitude in these machines, necessary for their functioning, is responsible for the appearance of a steady mass flow of the second order. Usually called streaming, it is superimposed on the first order oscillating acoustic mass flow. These dissipating energy phenomena have their origin in the nonlinear nature of the propagation. From energy considerations and despite their low level, these second order phenomena involve heat transfer to the wall, which is an undesirable loss mechanism. As acoustic streaming has been identified as an important source of energy dissipation in thermoacoustic devices [9–11], a better comprehension of this phenomenon is necessary for improving their performance.

By introducing the Reynolds stress tensor for acoustic waves, Lighthill was the first to attempt to describe the mechanisms at the origin of acoustic streaming [12]. The Reynolds tensor, well known in the theory of turbulence, has been extended to the theory of sound and can be written in the form, $\overline{\rho u_i u_j}$, where u_i are the fluctuating velocities in the sound and $\bar{\cdot}$ indicates the time average of the quantity underneath. Considering an area S oriented in the x_i direction, $\overline{\rho u_i u_j} S$ represents the time averaged transport of momentum in the x_i direction across S. As the Reynolds tensor acts as a stress, the difference between the force acting on the two opposite sides of a small block of fluid separated by a distance h generates a net force $-hS[\partial \overline{\rho u_i u_j}/\partial x_i]$. Per unit of volume, the ith component of the force acting on the fluid is

$$F_{Ri} = -\frac{\partial(\overline{\rho u_i u_j})}{\partial x_i}. \quad (1)$$

* Corresponding author. Tel.: +33 169858149.
E-mail address: kouidri@limsi.fr (S. Kouidri).

0011-2275/$ - see front matter © 2013 Elsevier Ltd. All rights reserved.
http://dx.doi.org/10.1016/j.cryogenics.2013.10.004

Nomenclature

c_0	speed of sound (m s^{-1})
$\mathrm{d}\dot{m}$	mass accumulation per unit of volume (kg m^{-3} s^{-1})
$\mathrm{d}\dot{M}$	mass accumulation in an elementary volume (kg s^{-1})
$\mathrm{d}\tau$	elementary volume (m^3)
F_R	volumic force induced by the spatial variation of the Reynolds stress tensor (N m^{-3})
F_{Ri}	ith component of the volumic force due to the spatial variation of the Reynolds stress tensor (N m^{-3})
F_{Ru}	first term of the volumic force due to the spatial variation of the Reynolds stress tensor (N m^{-3})
F_{Rv}	second term of the volumic force due to the spatial variation of the Reynolds stress tensor (N m^{-3})
F_μ	volumic force induced by the spatial variation of the viscous stress tensor (N m^{-3})
$F_{\mu i}$	ith component of the volumic force due to the spatial variation of the viscous stress tensor (N m^{-3})
k	wave number (m^{-1})
p	total pressure of the fluid (Pa)
p_a	acoustic pressure (Pa)
p_{a1}	first order of the acoustic pressure (Pa)
p_{a2}	second order of the acoustic pressure (Pa)
p_m	streaming pressure (Pa)
p_0	mean pressure (Pa)
R	width of the channel (m)
Re[ ]	real part
S	transverse section (m^2)
S_a	mass flow rate due to the propagation of the acoustic wave (kg m^{-3} s^{-1})
S_i	elementary surface of the volume oriented toward x_i (m^2)
T	total temperature of the fluid (K)
T_a	acoustic temperature (K)
T_{a1}	first order of the acoustic temperature (K)
T_0	mean temperature (K)
T_i	relative contributions of the streaming sources (%) $i = 1,2,3,4$
U	magnitude of the acoustic velocity (m s^{-1})
u_a	acoustic axial velocity (m s^{-1})
u_{ai}	ith component of the acoustic axial velocity (m s^{-1})
u_{a1}	first order of the acoustic axial velocity (m s^{-1})
u_i	ith component of the particle's velocity (m s^{-1})
u_L	average mass transport velocity (m s^{-1})
u_m	streaming axial velocity (m s^{-1})
v_a	acoustic transversal velocity (m s^{-1})
v_{a1}	first order of the acoustic transversal velocity (m s^{-1})
$\mathbf{v}$	particle's velocity (m s^{-1})
$\mathbf{v}_a$	acoustic velocity (m s^{-1})
$\mathbf{v}_{a1}$	first order of the acoustic velocity (m s^{-1})
$\mathbf{v}_{a2}$	second order of the acoustic velocity (m s^{-1})
$\mathbf{v}_m$	streaming velocity (m s^{-1})
x_i	ith coordinate (m)
x	axial coordinate (m)
y	transversal coordinate (m)
β	coefficient depending on the fluid
δ_{ik}	Kronecker delta
δ_v	thickness of the boundary layer (m)
η	dimensionless transversal coordinate
γ	ratio of heat capacity at constant pressure and constant volume
μ	shear viscosity (Pa s)
μ_{a1}	first order of the acoustic shear viscosity (Pa s)
μ_B	bulk viscosity (Pa s)
μ_0	mean shear viscosity (Pa s)
ω	angular frequency (s^{-1})
Ψ_i	complex functions dependent on the thermophysical properties of the fluid and geometric parameters, $i = 1,2,3$
ϕ_i	contributions of the streaming sources, $i = 1,2,3,4$ (m s^{-1})
ρ	total density of the fluid (kg m^{-3})
ρ_a	acoustic density (kg m^{-3})
ρ_{a1}	first order of the acoustic density (kg m^{-3})
ρ_{a2}	second order of the acoustic density (kg m^{-3})
ρ_m	streaming density (kg m^{-3})
ρ_0	mean density (kg m^{-3})
σ	Prandtl number
σ_{ik}	viscous stress tensor (Pa)

This force contributes to acoustic streaming generation [13].

Another well known mechanism at the origin of the secondary flow is the effect of viscosity. Considering an oscillating parcel of gas located at about the penetration depth from the wall, Olson and Swift described this phenomenon [14]. Due to thermal contact with the wall and the phasing between oscillatory pressure and motion, the gas between the parcel and the wall has a varying temperature during the oscillation. The parcel experiences differing amounts of viscous drag during its motion because the viscosity depends on the temperature. After a full cycle, the parcel does not return to its initial point. Bailliet et al. have developed a model describing streaming for standing waves and an arbitrary channel width, in which the temperature dependence of the viscosity is included [15]. In that model, the volumic force due to viscosity on the axial component x is

$$F_{\mu x} = \mathrm{div}_\eta(\overline{\mu \mathrm{grad}(u)}), \tag{2}$$

where x is the axial component and η is the transversal one. u is the x-component of the acoustic velocity and μ is the shear viscosity. The time average of this force is non-zero because the viscosity is time-dependent. The volumic force generated by the viscosity can be written in the form

$$F_{\mu i} = \frac{\partial \overline{\sigma_{ik}}}{\partial x_k}. \tag{3}$$

As for the Reynolds stress, the volumic force at the origin of streaming is due to a spatial variation of a stress tensor. The acoustic mass flow can also be a cause of streaming generation. The Reynolds stress, the viscosity, and the acoustic mass flow, identified as the phenomena at the origin of acoustic streaming will be quantified in a pressurised thermoacoustic primemover. Finally, the investigation on streaming sources will be extended to four channels with different widths.

2. Mechanisms of acoustic streaming generation

This section focuses on the mechanisms of acoustic streaming generation. The streaming equations are presented, discussed and solved. To investigate nonlinear effects in thermoacoustic devices, some assumptions are made. A secondary flow is assumed to be superimposed on the oscillating flow. The time and space dependent variables can be written in such a way as to take into account the variables in the absence of oscillations (ρ_0, p_0), acoustic variables ($\rho_a, p_a, \mathbf{v}_a$), and secondary flow variables ($\rho_m, p_m, \mathbf{v}_m$):

$$\rho = \rho_0 + \rho_a + \rho_m, \qquad p = p_0 + p_a + p_m, \qquad \mathbf{v} = \mathbf{v}_a + \mathbf{v}_m. \tag{4}$$

Each acoustic variable could be developed asymptotically:

$$\rho_a = \rho_{a1} + \rho_{a2} + \ldots, \quad p_a = p_{a1} + p_{a2} + \ldots, \quad \mathbf{v}_a = \mathbf{v}_{a1} + \mathbf{v}_{a2} + \ldots. \tag{5}$$

The acoustic Mach number is assumed to be much smaller than 1. The streaming is assumed to be stationary and the Mach number associated to the secondary flow is less than 0.3. Therefore, the secondary flow is expected to be incompressible. The Reynolds number of the streaming is significantly less than 1, so the advection term is negligible compared to the viscosity term. With this assumption, the corresponding secondary flow is called slow streaming. In this paper, the investigations focus on the Rayleigh streaming, and the mass flow through any cross section is zero in the steady-state operation. Under these assumptions, the equations governing the streaming at second order are [15]:

$$\rho_0 \left[\frac{\partial u_m}{\partial x} + \frac{\partial v_m}{\partial y} \right] = S_a, \tag{6}$$

$$0 = -\frac{\partial p_m}{\partial x} + \mu_0 \frac{\partial^2 u_m}{\partial y^2} + F_R + F_\mu, \tag{7}$$

$$\frac{\partial p_m}{\partial y} \sim 0, \tag{8}$$

where

$$S_a = -\left[\frac{\partial \overline{\rho_{a1} u_{a1}}}{\partial x} + \frac{\partial \overline{\rho_{a1} v_{a1}}}{\partial y} \right], \tag{9}$$

$$F_R = -\left[\frac{\partial \rho_0 \overline{u_{a1} u_{a1}}}{\partial x} + \frac{\partial \rho_0 \overline{v_{a1} u_{a1}}}{\partial y} \right], \tag{10}$$

$$F_\mu = \frac{\partial}{\partial y} \left[\overline{\mu_{a1} \frac{\partial u_{a1}}{\partial y}} \right]. \tag{11}$$

Eqs. (6)–(8) are the mass and momentum conservation equations governing the streaming, u_m and v_m are, respectively, the axial and the transversal velocity of the acoustic streaming, p_m is the additional pressure generated by the streaming, u_{a1} and v_{a1} are, respectively, the axial and the transversal acoustic velocity. As the shear viscosity depends on the temperature [16], it can be written as

$$\mu \propto T^\beta. \tag{12}$$

β is a coefficient depending on the fluid and μ_{a1} can be expressed as a function of T_{a1}

$$\mu_{a1} = \mu_0 \beta \frac{T_{a1}}{T_0}, \tag{13}$$

where T_{a1} is the additional temperature due to the acoustic wave. S_a, F_R, and F_μ are the acoustic streaming source terms, which are only governed by the acoustic field. F_R and F_μ are volumic forces due to, respectively, the spatial variation of the Reynolds tensor and that of the viscous stress tensor. F_R is composed of two terms:

$$F_{Ru} = -\frac{\partial \rho_0 \overline{u_{a1} u_{a1}}}{\partial x}, \tag{14}$$

$$F_{Rv} = -\frac{\partial \rho_0 \overline{v_{a1} u_{a1}}}{\partial y}. \tag{15}$$

The term S_a is a mass flow rate induced by the propagation of the acoustic wave. To understand the meaning of this term, it is assumed that there is no secondary flow. With this assumption, the density and the velocity are

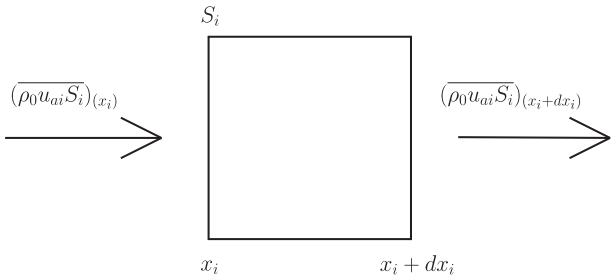

Fig. 1. Mass balance in an elementary volume $d\tau = dx_i\, dx_j\, dx_k$.

$$\rho = \rho_0 + \rho_{a1} \qquad u = u_{a1}. \tag{16}$$

The mass flow accumulated per unit of time inside an elementary volume $d\tau$ (Fig. 1) is

$$d\dot{M} = [\overline{\rho_{a1} u_{ai}}(x_i) - \overline{\rho_{a1} u_{ai}}(x_i + dx_i)] S_i = -\frac{\partial \overline{\rho_{a1} u_{ai}}}{\partial x_i} S_i dx_i \tag{17}$$

$S_i = dx_j dx_k|_{j,k \neq i}$ is an elementary surface of the volume $d\tau$. Per unit of volume, this mass accumulation becomes

$$d\dot{m} = \frac{d\dot{M}}{d\tau} = -\frac{\partial \overline{\rho_{a1} u_{ai}}}{\partial x_i} = S_a. \tag{18}$$

Without average flow, S_a represents a mass accumulation per unit of volume. As there is no accumulation, this mass is evacuated by generating a secondary flow, referred to as acoustic streaming.

To calculate the axial streaming velocity in a thermoacoustic device, the modeling of Bailliet et al. [15] was extended by incorporating the section variation. The solution of Eqs. (6)–(11) to second order gives an expression for the axial streaming velocity:

$$u_m = \phi_1 + \phi_2 + \phi_3 + \phi_4, \tag{19}$$

with

$$\phi_1 = \frac{3}{4\rho_0} (\eta^2 - 1) \int_{-1}^{1} \overline{\rho_{a1} u_{a1}} d\eta, \tag{20}$$

$$\phi_2 = \frac{R^2}{\mu_0} \left[\int_1^\eta \int_0^{\eta'} \frac{\partial (\rho_0 \overline{u_{a1} u_{a1}})}{\partial x} d\eta'' d\eta' - \frac{3}{4} (1 - \eta^2) \int_{-1}^{1} \int_1^\eta \int_0^{\eta'} \frac{\partial (\rho_0 \overline{u_{a1} u_{a1}})}{\partial x} d\eta'' d\eta' d\eta \right], \tag{21}$$

$$\phi_3 = \frac{R}{v_0} \left[\int_1^\eta \overline{u_{a1} v_{a1}}\, d\eta' - \frac{3}{4} (1 - \eta^2) \int_{-1}^{1} \int_1^\eta \overline{u_{a1} v_{a1}} d\eta' d\eta \right], \tag{22}$$

$$\phi_4 = -\frac{\beta}{T_0} \left[\int_1^\eta \left(\overline{T_{a1} \frac{\partial u_{a1}}{\partial \eta}} \right) d\eta' - \frac{3}{4} (1 - \eta^2) \int_{-1}^{1} \int_1^\eta \overline{T_{a1} \frac{\partial u_{a1}}{\partial \eta}} d\eta' d\eta \right]. \tag{23}$$

The contribution of the mechanisms mentioned previously are represented by ϕ_i in Eq. (19): ϕ_1, ϕ_2, ϕ_3, and ϕ_4 are, respectively, the contributions of the term S, F_{Ru}, F_{Rv}, and F_μ to the axial streaming velocity, and $\eta = y/R$ is the normalized transversal dimension. The centerline and the wall are respectively located at $\eta = 0$ and $\eta = 1$.

The acoustic variables are expressed in function of the acoustic pressure in a channel of non-constant section. The conservation equations of mass, momentum and energy and the state equation, solved in 2D Cartesian coordinates, yield the first order velocities, temperature and density:

$$u_{a1} = \frac{1}{i\omega\rho_0} F_\eta \frac{\partial p_{a1}}{\partial x} \tag{24}$$

$$T_{a1} = \frac{\gamma - 1}{\rho_0 c_0^2} T_0 F_{\eta t} p_{a1} - \frac{1}{\omega^2 \rho_0} \frac{F_{\eta t} - \sigma F_\eta}{1 - \sigma} \frac{\partial T_0}{\partial x} \frac{\partial p_{a1}}{\partial x} \tag{25}$$

$$\rho_{a1} = \frac{\gamma - (\gamma - 1) F_{\eta t}}{c_0^2} p_{a1} + \frac{1}{T_0 \omega^2} \frac{F_{\eta t} - \sigma F_\eta}{1 - \sigma} \frac{\partial T_0}{\partial x} \frac{\partial p_{a1}}{\partial x} \tag{26}$$

$$\begin{aligned} v_{a1} = {} & \frac{i\omega R}{\rho_0 c_0^2} \left(\gamma\eta + (1-\gamma)(\eta - \phi_t) + (\phi - \eta) \frac{\gamma + (1-\gamma) F_t}{F} \right) p_{a1} \\ & + \frac{iRb^2}{\omega\rho_0} \left((1 - F) \frac{\eta(F-1) + \phi}{F} \right) \frac{1}{R} \frac{\partial R}{\partial x} \frac{\partial p_{a1}}{\partial x} \\ & - \frac{iR}{\omega\rho_0} \left(b^2 (1 - F) \frac{\eta(F-1) + \phi}{F} + \eta F_\eta \right) \frac{\beta + 1}{2T_0} \frac{\partial T_0}{\partial x} \frac{\partial p_{a1}}{\partial x} \\ & + \frac{iR}{\rho_0 \omega (1 - \sigma)} (\eta - \phi_t + (\phi - \eta) F_t / F) \frac{1}{T_0} \frac{\partial T_0}{\partial x} \frac{\partial p_{a1}}{\partial x} \end{aligned} \tag{27}$$

where

$$b = \frac{(1-i)R}{\delta_v}, \quad \delta_v = \sqrt{\frac{2\mu_0}{\omega\rho_0}}, \tag{28}$$

$$\phi = \frac{\sinh(b\eta)}{b\cosh(b)}, \quad \phi_t = \frac{\sinh\left(\sqrt{\sigma} b\eta\right)}{b\sqrt{\sigma}\cosh\left(b\sqrt{\sigma}\right)} \tag{29}$$

$$F_\eta = 1 - \frac{\cosh(b\eta)}{\cosh b}, \quad F_t = 1 - \frac{\tanh\left(\sqrt{\sigma} b\right)}{\sqrt{\sigma} b}, \quad F = 1 - \frac{\tanh(b)}{b} \tag{30}$$

σ is the Prandtl number and γ is the ratio of heat capacity at constant pressure and constant volume. The expression of the axial velocity, the temperature and the density (24)–(26) are not modified with the consideration of a section variation [10,15,17].

The Eqs. (19)–(30) lead to an expression for the streaming axial velocity in terms of the control parameters:

$$\begin{aligned} u_m = {} & \frac{R^2}{\mu_0 \rho_0 c_0^2} \mathrm{Re}\left[\Psi_1 p_{a1} \left(\frac{\partial p_{a1}}{\partial x} \right)^* \right] + \frac{R^2}{\mu_0 \omega^2 \rho_0} \mathrm{Re}[\Psi_2] \frac{1}{R} \frac{\partial R}{\partial x} \left| \frac{\partial p_{a1}}{\partial x} \right|^2 \\ & + \frac{R^2}{\mu_0 \omega^2 \rho_0} \mathrm{Re}[\Psi_3] \frac{1}{T_0} \frac{\partial T_0}{\partial x} \left| \frac{\partial p_{a1}}{\partial x} \right|^2. \end{aligned} \tag{31}$$

where Ψ_1, Ψ_2 and Ψ_3 are complex functions depending on the thermo-physical properties of the fluid (its viscosity, density ...) the frequency and geometric parameters. Eq. (31) differs from the modeling of Bailliet et al. by the second term [15]. Indeed, this term takes into account the section variation. Eq. (31) associated with the knowledge of acoustic pressure allows to calculate the axial streaming velocity. The acoustic pressure could be calculated numerically by the software DeltaEC [18], so that no assumption is made on the type of wave, standing or progressive. Therefore, the combination of a numerical and an analytical modeling allows to determinate the axial velocity of slow streaming in every type of thermoacoustic device. Eq. (31) also allows highlighting three parameters which control the acoustic streaming: the spatial variation of the magnitude of the wave, $\frac{\partial p_{a1}}{\partial x}$, the section variation, $\frac{\partial R}{\partial x}$ and the temperature gradient, $\frac{\partial T_0}{\partial x}$. As the spatial variation of the magnitude of the wave is the major control parameter, no acoustic streaming is generated if the magnitude wave does not spatially change. For example, without viscous dissipation, the propagation of progressive waves does not generate acoustic streaming. As investigated previously by Olson and Swift, acoustic streaming could be locally suppressed by setting an adequate section variation. The theoretical values of acoustic streaming are obtained by Eq. (31).

3. Verification test

Before studying the mechanism of streaming generation, the theoretical fields are compared to the experimental values in a thermoacoustic prime mover for acoustic pressure, axial acoustic velocity and axial streaming velocity. A thermoacoustic-Stirling prime mover illustrated in Fig. 2 has been designed and built especially to investigate acoustic streaming. The experimental apparatus is composed of a closed loop and a straight resonance tube. This energy conversion system does not have any moving part, which increases its reliability [19]. Electric supply is used to bring heat to the hot heat exchanger and water stream passes through the cold heat exchanger. The 4.25-m-long resonator associated with the closed loop allows the system to work at the frequency of 22 Hz. The resonator is composed of three parts: a 56-mm-diameter tube connected by a tapered tube to a larger tube of 162 mm diameter. The system using nitrogen can operate up to a mean pressure of 30 bars. Kistler piezoelectric pressure sensors were flush mounted along the traveling wave engine allowing the acoustic pressure measurements. They are located from Cp1 to Cp8 positions. The measurements of acoustic and streaming velocity are performed by Laser Doppler Velocimetry (LDV). The system operates with a 600-nm-length-wave laser which delivers a power of 35 mW. The focus of the laser beams into the pressurised thermoacoustic prime mover is made through an optical device designed and built to resist to a pressure up to 40 bars. Two optical devices are placed on the thermoacoustic prime mover at the positions $x = 2.25$ m and $x = 3.52$ m. The acoustic flow is visualised by injecting particles of magnesium oxide into the system.

After setting the system at the desired pressure and supplying the heat exchanger, it is necessary to wait for the wave to reach its steady state. The time evolution of acoustic pressure represented on Fig. 3 shows that the transient state lasts approximately 90 min. $t = 0$ represents the moment of setting the supplier. The steady state is considered reached when the acoustic pressure has a variation less than 2% on a period of 10 min.

The acoustic pressure distribution along the resonator is represented on Fig. 4. Experimental data are compared to the theoretical results for 3 different mean pressures (a) and 3 different heat powers (b). The theoretical acoustic pressure is numerically calculated by DeltaEC. Although the channel has a circular section, the calculations are performed by a 2D-Cartesian model. Therefore, the surface curvature is assumed not to affect the studied phenomena. This assumption has already been used in the literature [20,21]. The theoretical results match the experimental ones with a relative error less than 6%, which validates the numerical modeling. The pressure nodes, depending only on the geometric configuration, are located at the position $x = 2.23$ m regardless the heat powers and the mean pressures. As the acoustic and streaming variables are expressed in function of the acoustic pressure and its derivative, the determination of the theoretical acoustic pressure field allows to calculate the acoustic and streaming velocities.

The theoretical velocities are represented by the lines in Fig. 5 for a mean pressure of 10 bars and three different heat powers: 165 W, 190 W and 210 W. They are compared to the experimental data performed by LDV and good agreements are observed. Concerning the acoustic streaming, as mentioned in the literatures [12], two different velocities could be used. The first velocity, expressed in Eulerian coordinates, is u_m obtained from Eq. (19). The second one, expressed in Lagrangian coordinates, is called the average mass transport velocity u_L. The relation between the Eulerian and the Lagrangian velocity is

$$u_L = u_m + \frac{\overline{\rho_{a1} u_{a1}}}{\rho_0} \tag{32}$$

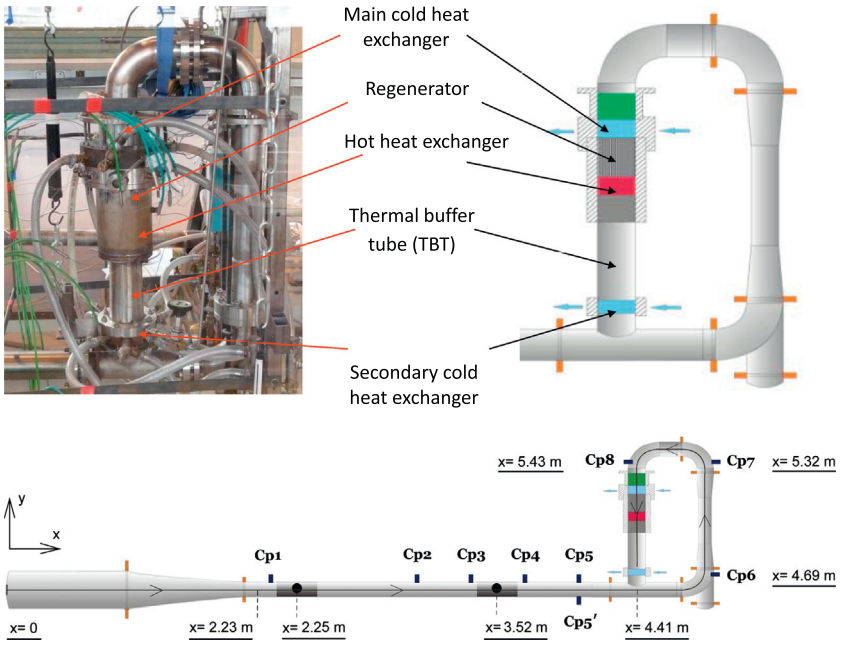

Fig. 2. Experimental setup.

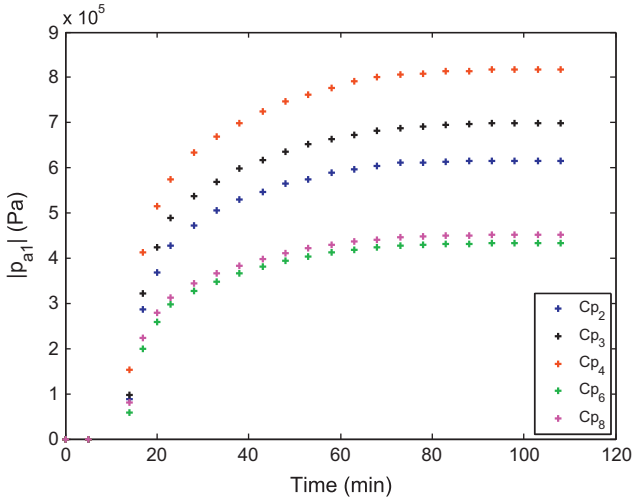

Fig. 3. Time evolution of the acoustic pressure.

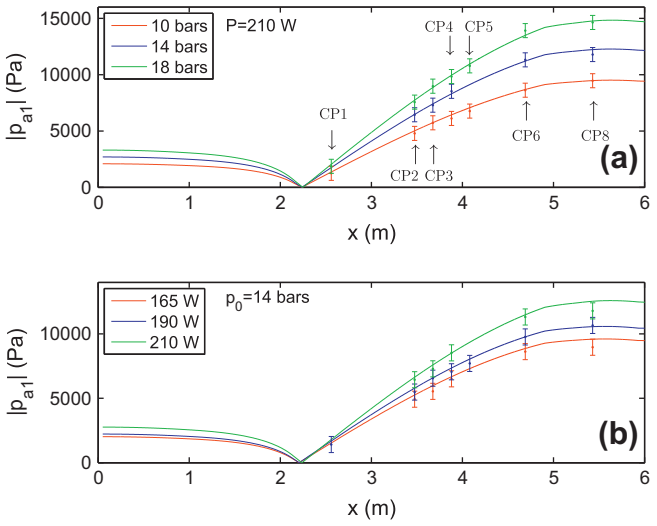

Fig. 4. Acoustic pressure distributions for a heat power of 210 W and three mean pressures 10, 14, 18 bars (a) and for a mean pressure of 10 bars and 3 heat powers 165 W, 190 W, 210 W (b). (—) Theory, (·) experimental values.

As the streaming velocity obtained with LDV techniques have to be compared with the Eulerian streaming velocity, u_m from Eq. (31) is plotted versus η in Fig. 5 for $x = 3.52$ m. The experimental data performed by LDV are represented in dot points. A good agreement is found between experimental and calculated results. This configuration allows to compare the order of the acoustic velocity with the streaming velocity; it is observed that the streaming velocity is two orders smaller than acoustic velocity. Similar results, not represented in this paper, are also obtained for all combinations of a mean pressure of 10, 14 and 18 bars with a heat power of 165 W, 190 W et 210 W.

4. Discussion

As the acoustic and streaming fields have been obtained and validated by experimental data, the influence of acoustic streaming sources can now be investigated. Thus, the different contributions are plotted versus η for $x = 3.52$ m on Fig. 6 for a mean pressure of 10 bars and a heat power of 210 W. The absolute contributions (a) are calculated using Eqs. (20)–(23) and the relative ones (b) are obtained by the following equation:

$$T_i = \frac{|\phi_i|}{|\phi_1| + |\phi_2| + |\phi_3| + |\phi_4|}. \tag{33}$$

Outside the boundary layer, the relative contributions maintain the same values whatever the location. In this configuration with a contribution equal to 92%, the Reynolds stress are the main mechanism of the streaming velocity generation. This result is in agreement with the theory of Rayleigh. Because Rayleigh neglected the temperature dependence of viscosity and considered that the streaming is divergence free, the streaming calculated by Rayleigh is only due to Reynolds stress ϕ_2 and ϕ_3:

$$u_{m\text{Rayleigh}} \sim \phi_2 + \phi_3 \tag{34}$$

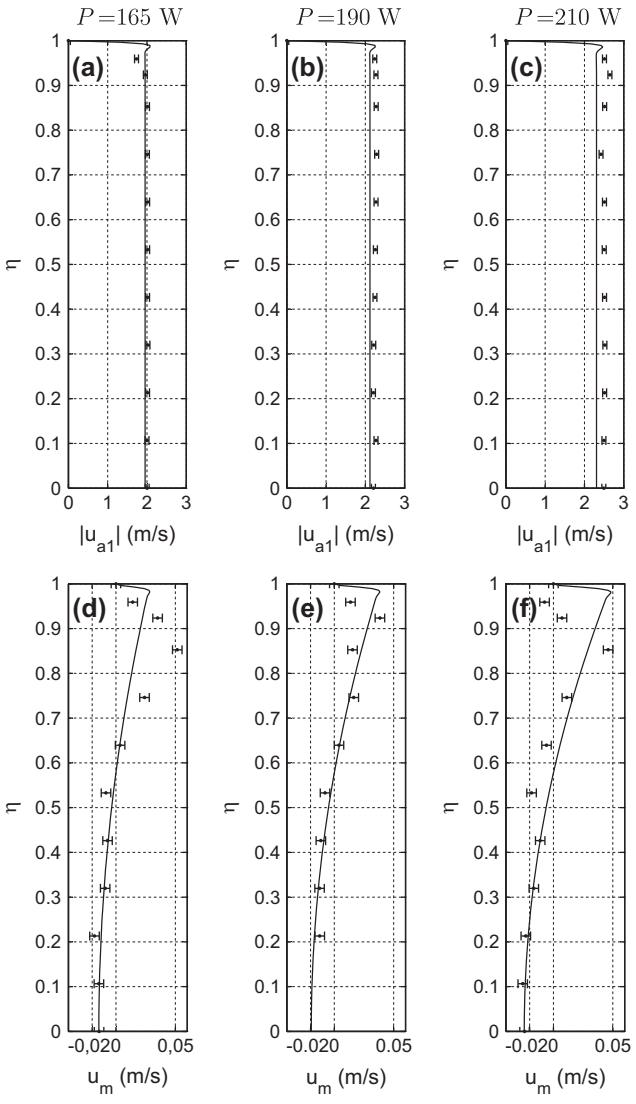

Fig. 5. Acoustic and streaming velocity profiles for a mean pressure of 10 bars and three differents heat powers: 165 W, 190 W and 210 W. (—) Theory, (·) LDV measurements.

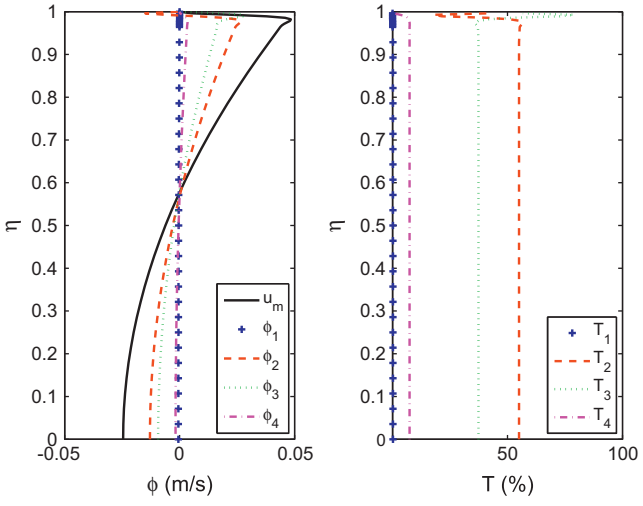

Fig. 6. Contributions of streaming velocity versus η for $x = 1.62$ m (a), and versus x for $\eta = 0$ (b). (···) ϕ_1, (---) ϕ_2, (···) ϕ_3, (-·-) ϕ_4.

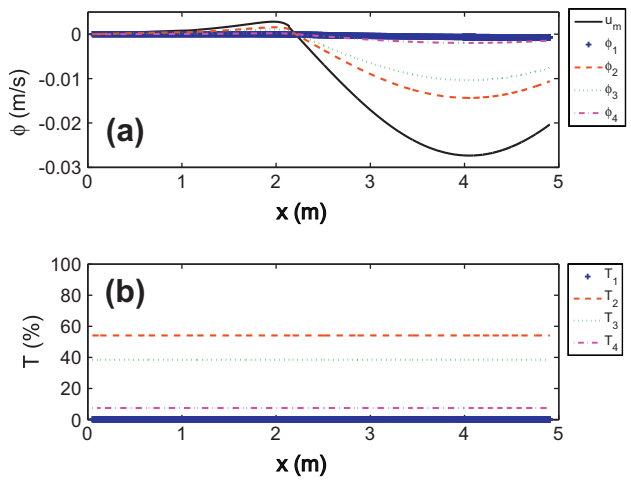

Fig. 7. Absolute (a) and relative (b) contributions of streaming velocity versus x for $\eta = 0$. (···) ϕ_1, (---) ϕ_2, (···) ϕ_3, (-·-) ϕ_4.

As his modeling predicts in a meaningful way the streaming velocity in a wide channel, it is coherent to find that the major source of streaming generation is due to Reynolds stress in our configuration. In our case, for $R/\delta_v = 360, T_1, T_2, T_3$, and T_4 make, outside of the boundary layer, a contribution of, respectively, 1%, 55%, 37%, and 7%. Similar values are also obtained for mean pressures of 10, 14 and 18 bars and heat powers of 165 W, 190 W and 210 W. The values of the relative contributions seem not depending on the magnitude of the acoustic wave.

Also investigated versus x, the absolute (a) and relative (b) contributions are plotted in Fig. 7 for $\eta = 0$, a mean pressure of 10 bars and a heat power of 210 W. The relative contributions maintain the same values whatever the location. The velocities vanish at the position $x = 0$, corresponding to the condition without penetration into the wall, and at the position $x = 2.23$ m, corresponding to the acoustic pressure node. The axial acoustic velocity is oriented towards the increasing x from 0 to 2.23 m to change direction between 2.23 m and 4.41 m. Therefore, in the whole resonator, the streaming velocity for $\eta = 0$ is always oriented towards the acoustic pressure node. This result is in agreement with the investigation of Hamilton et al. [22]. As the acoustic pressure has a higher amplitude from 2.23 m to 4.41 m than that from 0 to 2.23 m (Fig. 4), similar result is observed for streaming velocity. The influence of the

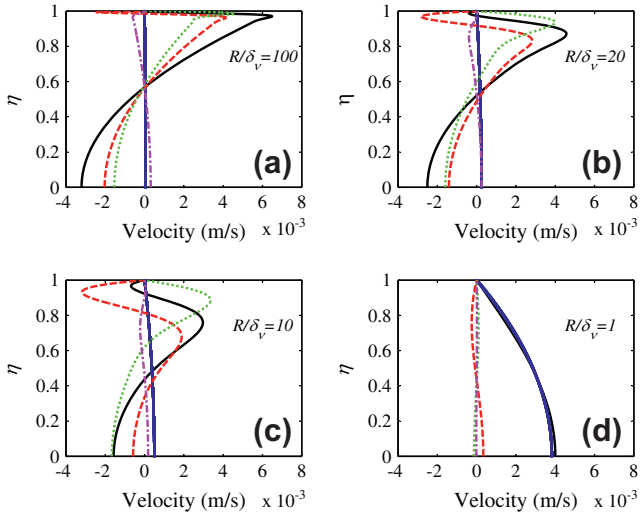

Fig. 8. Streaming velocity and its contributions versus η for different channel widths. (—) u_m, (···) ϕ_1, (---) ϕ_2, (···) ϕ_3, (-·-) ϕ_4.

section variation on the streaming velocity, represented by the second term of Eq. (31), could not be seen on Fig. 7 as in this case the tapered tube is located at the vicinity of the acoustic pressure node $x = 2.23$ m. The Rayleigh vortex is located at this position and the axial streaming velocity is almost zero.

In order to understand the physical interpretation of the different contributions, the present study was carried further: the influence of the channel width on the acoustic streaming was analysed. The study was performed in a 1 m long rectangular resonator subjected to a standing wave. In the resonator, the mean pressure is 10^6 Pa and the mean temperature is 293 K. The wave frequency is 170 Hz, a resonant frequency of the device functioning with air. The pressure magnitude is chosen to be 10^5 Pa. The investigations were made versus the ratio R/δ_v as this is a pertinent parameter with which to quantify the channel width.

In Fig. 8, the axial acoustic streaming (u_m) and its contributions ($\phi_1, \phi_2, \phi_3, \phi_4$) are plotted versus $\eta = y/R$ for R/δ_v equal to 100, 20, 10, and 1. As inner streaming is delimited by a succession of a maximum and a minimum of the velocity, an increase is observed when R/δ_v decreases from 100 to 10. The inner streaming is due to ϕ_2 as the sequence of a maximum then a minimum appears only for the first component of the Reynolds stress. Unlike inner streaming, outer streaming is characterized by a sequence of a local minimum then a local maximum. This sequence appears for ϕ_2 and ϕ_3. Outer streaming is due to the Reynolds stress. Because both inner and outer streamings are due to the Reynolds stress, they naturally disappear for $R/\delta_v = 1$ when ϕ_1 becomes predominant (Fig. 8 (d)).

5. Conclusion

Acoustic streaming has been investigated in a pressurised thermoacoustic prime mover. To calculate acoustic streaming, the equations were solved to take into account the section variation. Then, measurements of the streaming velocity were made and compared with the theoretical values. The experimental values fit the model which allowed the validation of the theory. Then, the mechanisms of streaming generation were investigated. Three phenomena causing the acoustic streaming have been identified: acoustic mass flow, Reynolds stress, and viscosity. Their physical interpretations have been given and their contributions have been evaluated. The mechanism of mass flow is found to be the main contribution of acoustic streaming velocity in narrow ducts whereas the major contribution in large channel is due to Reynolds stress. When the channel width is decreasing, the proportion of inner streaming is increasing. Because inner and outer streaming is due to Reynolds stress, at a certain limit when the channel is too narrow, there is no inner and outer streaming. This investigation and the understanding of the origins of streamings are an important step in improving the energetic performance of thermoacoustic systems.

Acknowledgements

The authors would like to thank H. Bailliet, I. Reyt and C. Valière from the Pôle Poitevin de Recherche pour l'Ingénieur en Mécanique, Matériaux et Energétique for sharing their expertise on acoustic streaming measurements. The authors also acknowledge Prof. T. Jin for the valuable discussions and for revising the manuscript.

References

[1] Backhaus S, Swift GW. A thermoacoustic Stirling heat engine. Nature 1999;399:335–8.
[2] Herman C. Thermoacoustic refrigeration: low-temperature applications and optimization. Low Temp Cryogenic Refrig 2003;99:327–48.
[3] Hariharan NM, Sivashanmugam P, Kasthurirengan S. Experimental investigation of a thermoacoustic refrigerator driven by a standing wave twin thermoacoustic prime mover. Int J Refrig 2013. http://dx.doi.org/10.1016/j.ijrefrig.2013.04.017.
[4] Tang K, Bao R, Chen G, Qiu Y, Shou L, Huang Z, et al. Thermoacoustically driven pulse tube cooler below 60 K. Cryogenics 2007;47(9):526–9.
[5] Jin T, Chen G, Shen Y. A thermoacoustically driven pulse tube refrigerator capable of working below 120 K. Cryogenics 2001;41(8):595–601.
[6] Tang K, Chen G, Jin T, Bao R, Li X. Performance comparison of thermoacoustic engines with constant-diameter resonant tube and tapered resonant tube. Cryogenics 2006;46(10):699–704.
[7] Tijani MEH, Spoelstra S. A high performance thermoacoustic engine. J Appl Phys 2011;42(1):110–6.
[8] Chaitou H, Nika P. Exergetic optimization of a thermoacoustic engine using the particle swarm optimization method. Energy Conver Manage 2012;55:71–80.
[9] Hu J, Luo E, Wu Z, Dai W, Zhu S. Investigation of an innovative method for dc flow suppression of double-inlet pulse tube coolers. Cryogenics 2007;47(5):287–91.
[10] Gusev V, Job S, Bailliet H, Lotton P, Bruneau M. Acoustic streaming in annular thermoacoustic prime-movers. J Acoust Soc Am 2000;108:934–45.
[11] Swift GW, Gardner D, Backhaus S. Acoustic recovery of lost power in pulse tube refrigerators. J Acoust Soc Am 1999;105:711–24.
[12] Lighthill J. Acoustic streaming. J Sound Vibr 1978;61(3):391–418.
[13] Valdes LC, Santens D. Influence of permanent turbulent air flow on acoustic streaming. J Sound Vibr 2000;230(1):1–29.
[14] Olson J, Swift GW. Acoustic streaming in pulse tube refrigerators: tapered pulse tubes. Cryogenics 1997;37(12):769–76.
[15] Bailliet H, Gusev V, Raspet R, Hiller R. Acoustic streaming in closed thermoacoustic devices. J Acoust Soc Am 2001;110:1808–21.
[16] Rott N. Thermoacoustics. Adv Appl Mech 1980;20:135–75.
[17] Arnott WP, Bass HE, Raspet R. General formulation of thermoacoustics for stacks having arbitrarily shaped pore cross sections. J Acoust Soc Am 1991;90:3228.
[18] Ward B, Clark J, Swift GW. Design environment for low-amplitude thermoacoustic energy conversion, DeltaEC version 6.2: Users guide; 2008.
[19] Backhaus S, Swift GW. A thermoacoustic-Stirling heat engine: detailed study. J Acoust Soc Am 2000;107:3148–66.
[20] Moreau S, Bailliet H, Valière J. Measurements of inner and outer streaming vortices in a standing waveguide using laser doppler velocimetry. J Acoust Soc Am 2008;123:640.
[21] Thompson M, Atchley A. Simultaneous measurement of acoustic and streaming velocities in a standing wave using laser Doppler anemometry. J Acoust Soc Am 2005;117:1828.
[22] Hamilton MF, Ilinskii YA, Zabolotskaya EA. Thermal effects on acoustic streaming in standing waves. J Acoust Soc Am 2003;114:3092–101.